Hindered Transport of Macromolecules in Isolated Glomeruli. I. Diffusion Across Intact and Cell-Free Capillaries

Aurélie Edwards,* William M. Deen,* and Barbara S. Daniels#
*Department of Chemical Engineering, Massachusetts Institute of Technology, Cambridge, Massachusetts 02139, and #Department of Medicine, University of Minnesota, Minneapolis, Minnesota 55455 USA

ABSTRACT The filtrate formed by renal glomerular capillaries must pass through a layer of endothelial cells, the glomerular basement membrane (GBM), and a layer of epithelial cells, arranged in series. To elucidate the relative resistances of the GBM and cell layers to movement of uncharged macromolecules, we measured the diffusional permeabilities of intact and cell-free capillaries to narrow fractions of Ficoll with Stokes-Einstein radii ranging from 3.0 to 6.2 nm. Glomeruli were isolated from rat kidneys, and diffusion of fluorescein-labeled Ficoll across the walls of single capillary loops was monitored with a confocal microscopy technique. In half of the experiments the glomeruli were treated first to remove the cells, leaving skeletons that retained the general shape of the glomerulus and consisted almost entirely of GBM. The diffusional permeability of cell-free capillaries to Ficoll was ~10 to 20 times that of intact capillaries, depending on molecular size. Taking into account the blockage of much of the GBM surface by cells, the contribution of the GBM to the diffusional resistance of the intact barrier was calculated to be 13% to 26% of the total, increasing with molecular size. Thus, the GBM contribution, although smaller than that of the cells, was not negligible. The structure that is most likely to be responsible for the cellular part of the diffusional resistance is the slit diaphragm, which spans the filtration slit between epithelial foot processes. A novel hydrodynamic model was developed to relate the diffusional resistance of the slit diaphragm to its structure, which was idealized as a single layer of cylindrical fibers in a ladder-like arrangement.

INTRODUCTION

The first step in urine formation in the kidney is the ultrafiltration of blood in the glomerular capillaries. The walls of these capillaries are an exquisitely "well-engineered" barrier, which is normally very permeable to water and yet able to prevent all but very minute losses from the circulation of serum albumin and the other major plasma proteins. As reviewed by Maddox et al. (1992), the selectivity of the glomerular capillary wall to macromolecules is normally based on both molecular size and molecular charge, and is also influenced by molecular shape. In the major forms of kidney disease this macromolecular selectivity is compromised, resulting in increased amounts of protein in the glomerular filtrate and the consequent appearance of much of that protein in the urine (proteinuria). It is important to elucidate the structural elements of the glomerular capillary wall responsible for normal barrier function, and the alterations responsible for proteinuria. The glomerular capillary wall consists of three distinct layers, as shown schematically in Fig. 1. Going outward from the capillary lumen, there is a fenestrated endothelium, the glomerular basement membrane (GBM), and a layer formed by the foot processes of glomerular epithelial cells. The filtration slits between adjacent podocytes are bridged by thin slit diaphragms. The high rate of water filtration suggests that the filtrate pathway is extracellular rather than transcellular. That is, the filtrate is thought to pass through the endothelial fenestrae, across the GBM, and then through the slit diaphragms and filtration slits.

The permeability properties of the glomerulus have been studied in vivo by micropuncture and fractional clearance techniques (Maddox et al., 1992). Glomerular micropuncture, which is applicable only to laboratory animals, measures single-nephron glomerular filtration rate and allows calculation of the glomerular ultrafiltration coefficient (the product of the hydraulic permeability of the barrier and the surface area for filtration). The macromolecular permeability of the barrier in humans or animals is assessed by measuring the fractional clearance of exogenous test macromolecules of varying size and charge; for test solutes that are neither reabsorbed nor secreted by the renal tubules, the fractional clearance (the clearance of the solute divided by that of inulin, a marker for water) is equal to the filtrate-to-plasma concentration ratio. This approach has also been used to study the macromolecular permeability of isolated, perfused, whole kidneys. Whereas these techniques measure the overall permeability characteristics of the capillary wall, in vitro approaches using either isolated capillaries or parts of the capillary wall are needed to quantitate the contributions of the individual layers.

Confocal microscopy has been used to assess the diffusion of fluorescent dextran across optical cross sections of single capillary loops of isolated glomeruli (Daniels et al., 1993). The technique has been applied to intact glomeruli and to glomeruli treated with a detergent to remove cells, leaving a skeleton of GBM. Using a polydisperse fluorescein-dextran as the test molecule, it was found that the cells

Received for publication 1 April 1996 and in final form 2 October 1996.
Address reprint requests to Dr. William M. Deen, Department of Chemical Engineering, Room 66-509, Massachusetts Institute of Technology, 77 Massachusetts Avenue, Cambridge, MA 02139-4307. Tel.: 617-253-4535; Fax: 617-258-8224; E-mail: wmdeen@mit.edu.

0006-3495/97/01/204/10 $2.00

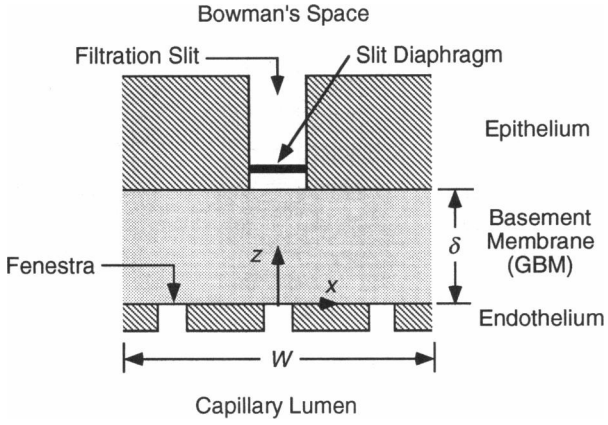

FIGURE 1 Idealized structural unit of the glomerular capillary wall. Indicated are the width of the structural unit (W) and the thickness of the GBM (δ). Filtration is in the z direction, from the capillary lumen to Bowman's space.

rather than the GBM offered the dominant resistance to diffusion. The objective of the present study was to extend those results by using macromolecules covering a range of well-defined sizes. Ficoll was selected because it is a more ideal test molecule than dextran, in that it appears to behave more nearly as a neutral, rigid sphere (Davidson and Deen, 1988; Oliver et al., 1992). Accordingly, four narrow fractions of fluorescein-Ficoll were prepared, and their rates of diffusion were measured in both intact and cell-free glomeruli. The results were interpreted using theoretical models for diffusion across components of the capillary wall. In the companion study (Edwards et al., 1997) additional methods were used to characterize the convective transport of Ficoll across GBM.

EXPERIMENTAL METHODS

Preparation of glomeruli

Adult male Sprague-Dawley rats weighing ~350 g were anesthetized with Inactin (100 mg/kg body weight), and both kidneys were perfused in situ at 110 mmHg with modified Eagle's medium (pH 7.4) to remove blood. The perfusion was completed within 10 s. The cortex was diced into 1-mm^3 bits and passed sequentially through 250-, 150-, and 75-μm pore-size nylon filters to isolate glomeruli. The isolation procedure was performed on ice in the presence of buffer with 5 mM pyruvate, 5 mM butyrate, and 1 mM alanine. As revealed by light microscopy, the resulting glomerular preparation contained >95% glomeruli and <5% tubular fragments. Over 95% of the glomeruli were devoid of Bowman's capsule and arterioles.

Diffusion studies were performed using both intact glomeruli and glomeruli from which the cells had been removed. Acellular glomeruli were prepared by incubating glomeruli with *N*-lauryl sarcosine to remove cells and DNAse to remove nucleoprotein, as described previously (Ligler and Robinson, 1977; Daniels et al., 1992). The resulting glomerular skeletons maintained the general shape of the glomerulus and were composed predominantly of GBM, with a few areas of residual mesangial matrix. Immunofluorescence microscopy of GBM obtained in that manner has confirmed the presence of laminin, type IV collagen, and heparan sulfate proteoglycan (Daniels et al., 1992).

We have previously demonstrated that both the core protein and sulfated side chains of heparan sulfate proteoglycan are present, that there is not histone binding to the GBM, and that alternative GBM isolation techniques yield similar results (Daniels, 1994).

Confocal microscopy apparatus

Diffusional permeabilities of intact or cell-free capillary loops to fluorescein-labeled macromolecules were measured with a confocal microscope (model ACAS 570; Meridian Instruments, Okemos, MI) as described by Daniels et al. (1993). A 5-W argon laser (Coherent Inova 90-5) was the source for fluorescence excitation. An Olympus epifluorescence inverted microscope was equipped to obtain either phase-contrast or fluorescent images. A pinhole limited the entrance of light to the photodetector to that originating from within the plane of focus and was adjustable to facilitate variations of optical section thickness. For these studies, a pinhole of 225 μm was used to produce a section thickness of about 1 μm. A 28-μm line was scanned at a step size of 0.4 μm and a peak velocity of 0.4 mm/s, using a laser power of approximately 3 mW. Each point was sampled eight times, the first time for 8 μs and subsequent samplings for 4 μs, so that the total laser exposure time was 36 μs. Approximately 30% of the laser power was present in the 488-nm line (the excitation wavelength used), so that about 0.9 mW of laser power was transmitted to the sample. All laser parameters were set to limit photobleaching to less than 5% loss of the initial fluorescence per 100 scans. Images were stored digitally on Bernoulli disks and subsequently analyzed with image analysis software integral to the ACAS system.

Macromolecules

Four narrow fractions of Ficoll, with Stokes-Einstein radii (r_s) of 3.0, 3.8, 4.8, and 6.2 nm, were obtained by special order from Pharmacia LKB (Piscataway, NJ). These samples were labeled with fluorescein and characterized as described previously (Johnson et al., 1996). The values of the polydispersity index (ratio of weight-averaged to number-averaged molecular weight) ranged from 1.13 to 1.22, as determined by the manufacturer. The number of fluoresceins per Ficoll molecule was estimated to be less than three, so that the negative charge resulting from the fluorescein label was assumed to be negligible.

Permeability measurements

Diffusional permeabilities were measured using the procedure described by Daniels et al. (1993). Intact or acellular glomeruli were incubated at 27°C for 20 min in a buffer solution containing 2 mg/ml of one of the fluorescein-Ficoll fractions. The buffer consisted of Dulbecco's modified Eagle's medium (25 mM HEPES) with 5 mM butyrate, 5 mM alanine, and 5 mM pyruvate substituted for equimolar NaCl. This resulted in diffusional equilibration of Ficoll between the bath and the capillary lumen. Glomeruli were then placed in a coverglass chamber (Nunc, Naperville, IL) and immobilized with a weighted nylon mesh to minimize movement during the scans. A longitudinal section of glomerular capillary without an overlying epithelial cell body was located by phase-contrast microscopy, and a plane of focus through the maximal diameter of the capillary was selected for ease in repeated identification of the original place of focus. An initial fluorescent scan was obtained to quantitate intracapillary fluorescence. The background fluorescence was then rapidly decreased by diluting the bathing fluid with Ficoll-free buffer; this resulted in a 75% decrease in bath fluorescence over 2 s. Although the change in bath concentration required only a few seconds, the first scan was delayed by about 120 s to confirm the original plane of focus. Because the diffusion of Ficoll was very rapid across acellular glomeruli, only glomeruli that did not move during the buffer change were used. The decline in fluorescence within the capillary was assessed by obtaining confocal images every 20–40 s. The bath fluorescence usually remained constant because of the large bath volume relative to intraglomerular or intracapillary volume. The lumen and bath fluoresence were characterized by the mean pixel fluorescence for 7 and 17 μm lines, respectively, typically separated by a distance of 7 μm. The

number of experiments performed for each of the 8 combinations of molecular size and barrier type ranged from 7 to 11.

The capillary lumen and the bath (corresponding to Bowman's space in vivo) were assumed to be well-mixed compartments separated by a membrane of surface area A.

Because the bath concentration (C_B) remained constant during the period of observation, the mass-balance equation governing the concentration in the lumen (C_L) is

$$\frac{dC_L}{dt} = -\frac{kA}{V_L}(C_L - C_B), \quad (1)$$

where V_L is the volume of the luminal compartment and k is the diffusional permeability of the intact or acellular capillary wall for the test solute ($k = k_{wall}$ and $k = k_{bare}$, respectively). For a capillary segment of radius R and length L, the surface-to-volume ratio is $A/V_L = 2/R$. Integration of Eq. 1 gives

$$\ln\left[\frac{C_L(t) - C_B}{C_L(0) - C_B}\right] = -\frac{2kt}{R}. \quad (2)$$

The value of k/R was obtained from the slope of a semilogarithmic plot of the bracketed concentration ratio versus time. The capillary radius R was determined using the image analysis software, allowing calculation of k.

THEORY

Diffusional permeability of the GBM

The GBM was modeled as a homogeneous, isotropic material. Accordingly, for the pseudo-steady conditions of our experiments, the concentration (C) of any solute was assumed to be governed by Laplace's equation,

$$\nabla^2 C = 0. \quad (3)$$

Referring to the idealized structural unit shown in Fig. 1, the boundary conditions used were $\mathbf{n} \cdot \nabla C = 0$ at the cell surfaces and planes of symmetry, and $\mathbf{n} \cdot \nabla C$ equal to specified constants on the areas occupied by endothelial fenestrae and epithelial filtration slits, where $\mathbf{n}$ is a unit vector normal to the boundary. The mathematical problem just described is identical to that for water flow governed by Darcy's law; in that case the pressure replaces C. Accordingly, an analytical solution derived previously for the water-flow problem (equation 21 of Drumond and Deen, 1994a) was used to compute k_{GBM} from k_{bare}. The parameters involved are the ratio of the GBM thickness to the width of the structural unit (δ/W), the number of fenestrae per structural unit (N_f), and the fractional areas occupied by the fenestrae (ϵ_f) and slits (ϵ_s). Values representative of glomerular capillaries in normal rats are $\delta/W = 0.56$, $N_f = 3$, $\epsilon_f = 0.20$, and $\epsilon_s = 0.11$ (Drumond and Deen, 1994a). For these inputs it was found that $k_{bare}/k_{GBM} = 2.33$.

Diffusional permeability of the slit diaphragm

The slit diaphragm has been shown to have a fibrous structure that makes it a likely candidate to present the major part of the cellular resistance. Fig. 2 shows two possible representations of this structure. The widely quoted study of Rodewald and Karnovsky (1974) shows a central filament

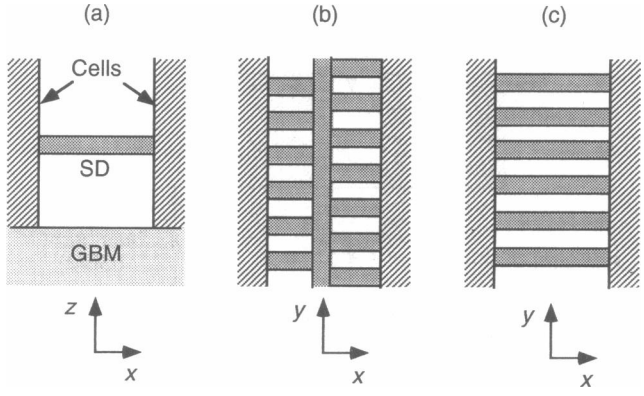

FIGURE 2 Representations of the epithelial slit diaphragm. (*a*) A view perpendicular to the direction of flow, as in Fig. 1. (*b*) A view parallel to the direction of flow, showing the structure proposed by Rodewald and Karnovsky (1974), the "zipper" configuration. (*c*) Another view parallel to the direction of flow, showing the "ladder" configuration.

connected to the podocytes by cylindrical "bridge" fibers, leaving open spaces comparable to the dimensions of an albumin molecule (4 × 14 nm), a "zipper" structure. An alternative, suggested by the results of Hora et al. (1990), consists of a row of parallel cylinders, a "ladder structure." Although the two structures differ in detail, they share the important feature that permeating macromolecules must pass through a single row of cylindrical fibers, in which the smallest dimension of the opening is the distance between adjacent cylinders. We explore the hypothesis that the slit diaphragm accounts for essentially all of the cellular part of the diffusional resistance, just as it has been shown to account for virtually all of the cellular resistance to the glomerular filtration of water (Drumond and Deen, 1994a). A corollary to this hypothesis is that the diffusional resistance of the endothelial fenestrae is equivalent, at most, to that of a slight increase in the thickness of the GBM.

We adapted the hydrodynamic model used by Drumond and Deen (1995) to describe convective movement of macromolecules through the filtration slit and slit diaphragm. The model used here for diffusion estimates the increased hydrodynamic drag, and the consequent reduction in the local mobililty or diffusivity, which is experienced by a spherical macromolecule moving through a single row of closely spaced cylinders. To simplify the computations, only the ladder geometry was considered. The primary geometric parameters are illustrated in Fig. 3. They are the solute radius (r_s), the radius of the cylinders that constitute the slit diaphragm (r_c), and the center-to-center spacing of the cylinders ($2L$). A more useful measure of cylinder spacing for some purposes is the opening half-width, given by $u = L - r_c$. It was found that, unless u is very large, the diffusional resistance of the slit diaphragm greatly exceeds that of the remainder of the slit channel.

The slit diaphragm, which was modeled initially as a row of long, equally spaced cylinders, was treated separately from the slit channel. The key aspect of this diffusional

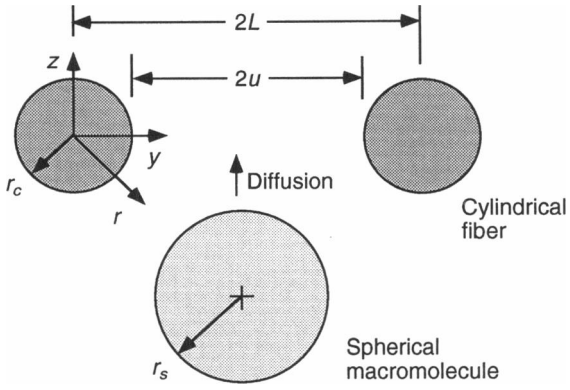

FIGURE 3 Coordinates used in modeling diffusion of macromolecules through the slit diaphragm.

problem is that hydrodynamic interactions with the cylinders cause the diffusivity of a spherical macromolecule to depend on both its position and its direction of movement. Accordingly, the scalar diffusivity D_∞ must be replaced by a position-dependent tensor. Using the dimensionless tensor $\mathbf{d}$ computed by Drumond and Deen (1995), which is defined such that the diffusivity is given by $D_\infty\mathbf{d}$, the steady concentration field is governed by

$$\nabla \cdot (\mathbf{d} \cdot \nabla C) = 0. \tag{4}$$

Equation 4, subject to the boundary conditions stated below, was solved using a Galerkin finite-element method, with quadrilateral elements and bilinear basis functions. With reference to the coordinates and dimensions shown in Fig. 3, the boundary conditions used were

$$\mathbf{e}_z \cdot (\mathbf{d} \cdot \nabla C) = -J_0/D_\infty \quad \text{at } z \to -\infty \tag{5}$$

$$C = C_0 \quad \text{at } z \to +\infty \tag{6}$$

$$\mathbf{e}_y \cdot (\mathbf{d} \cdot \nabla C) = 0 \quad \text{at } y = 0 \text{ and } y = L \tag{7}$$

$$\mathbf{e}_r \cdot (\mathbf{d} \cdot \nabla C) = 0 \quad \text{at } r = r_c + r_s, \tag{8}$$

where $\mathbf{e}_j$ is a unit vector directed along coordinate j. Equation 5 specifies a constant flux J_0 far upstream from the cylinders, and Eq. 6 sets a constant concentration C_0 far downstream. It was found that $z = \pm 15L$ was large enough to approximate $\pm\infty$ in all cases. That is, applying the upstream and downstream conditions farther away had a negligible effect on the results. Equations 7 and 8 state that the solute flux normal to the boundary of the domain is zero at the symmetry planes ($y = 0$ and $y = L$) and where a sphere contacts a cylinder ($r = r_c + r_s$).

The permeability for a row of uniformly spaced cylinders, k_{cyl}, was defined as

$$k_{cyl} = \frac{J_0}{(\Delta C)_{cyl}}, \tag{9}$$

where $(\Delta C)_{cyl}$ is the concentration drop in the z direction above that corresponding to a uniform flux J_0 and a constant diffusivity D_∞. The results for various combinations of the geometric parameters were correlated in terms of the dimensionless mass transfer coefficient, or Sherwood number (Sh), defined by

$$Sh = \frac{k_{cyl} r_s}{D_\infty}. \tag{10}$$

The Sherwood number could be expressed as a function of just two dimensionless quantities, r_c/L and r_s/u, where $u = L - r_c$. For convenience in other calculations, the results were fitted by an empirical formula,

$$Sh = \frac{A(1 - [r_s/u])^B(1 - [r_c/L])^C(r_c/L)^D}{1 + (r_s/u)^E(r_c/L)^F}, \tag{11}$$

which was chosen to give the correct limit of $Sh \to 0$ for $r_c/L \to 1$ or $r_s/u \to 1$. Results were obtained for $0.1 \le r_c/L \le 0.9$ and $0.1 \le r_s/u \le 0.95$, for a total of 306 values of Sh. Powell's method (Press et al., 1989) was used to find the constants in Eq. 11, giving $A = 0.111$, $B = 0.795$, $C = 1.138$, $D = 0.080$, $E = -0.883$, and $F = 3.731$. Equation 11 represented the numerical results very accurately, with a root mean square error of only 3.9%.

Nonuniformities in the structure of the slit diaphragm were modeled by assuming a lognormal distribution of cylinder spacings. The probability density function $g(u)$ for the gap half-width u was written as

$$g(u) = \frac{1}{\sqrt{2\pi}\, u \ln s} \exp\left[-\frac{1}{2}\left(\frac{\ln(u/u_m)}{\ln s}\right)^2\right], \tag{12}$$

where u_m is the mean value of u and $\ln s$ is the standard deviation. To determine the average permeability for the slit diaphragm, k_{sd}, the results were integrated over the distribution of spacings. The average permeability for a given solute size was calculated as

$$\frac{k_{sd} r_s}{D_\infty} = \frac{\int_0^\infty Sh(u)(r_c + u)g(u)\mathrm{d}u}{\int_0^\infty (r_c + u)g(u)\mathrm{d}u}. \tag{13}$$

The weighting factor, $(r_c + u) = L$, comes from the fact that the solute flux must be integrated over the total cross-sectional area of the slit diaphragm; the area of a single unit (pair of adjacent cylinders) is proportional to L. The integrals in Eq. 13 were evaluated using Romberg's method (Press et al., 1989).

Diffusional permeability of the slit channel

The filtration slit between adjacent podocytes was modeled as a channel bounded by flat, parallel walls, with a half-width h and length H. Electron micrographs indicate that, in reality, the slit generally tapers outward as one moves away from the basement membrane. That is, the half-width is smaller at the upstream end (h_{min}) than at the downstream end (h_{max}). To simplify the final model for the slit, we replaced the tapered channel by a parallel-wall channel that has an equivalent diffusional permeability. This was done

by setting $h = h_{min}$, and computing the value of H that gave results equivalent to those for a channel where the half-width varies linearly from h_{min} to h_{max} over an actual length H_0. A consequence of choosing $h = h_{min}$ is that $H < H_0$.

The diffusional permeability of a tapered channel was computed by solving Eq. 3, with a constant flux at the upstream end, a constant concentration at the downstream end, and no flux normal to the walls. The Galerkin finite-element method was used, with quadrilateral elements and bilinear basis functions. Results were obtained for $h_{min} = 20$ nm, $60 \leq h_{max} \leq 110$ nm, and $200 \leq H_0 \leq 400$ nm, corresponding to approximate ranges of values estimated from electron micrographs. The results were fitted to the expression

$$\frac{H}{H_0} = \left(\frac{h_{max}}{h_{min}}\right)^c \exp\left[a\left(\frac{h_{max}}{h_{min}} - 1\right)^b\right], \quad (14)$$

which ensures that $H/H_0 \rightarrow 1$ as $h_{max}/h_{min} \rightarrow 1$. Using Powell's method (Press et al., 1989), the best-fit values for the constants were found to be $a = -0.7010$, $b = 0.6511$, and $c = -0.4426$. The root mean square error for 121 cases was 0.8%. Choosing $h_{max} = 90$ nm and $H_0 = 300$ nm as most representative of the actual shape, Eq. 14 gives $H = 132$ nm.

Hindered diffusion of a spherical macromolecule through a parallel-plate channel has been analyzed by Pawar and Anderson (1993). Their result for the diffusivity, denoted here as D_{sc}, is

$$\frac{D_{sc}}{D_\infty} = 1 + \frac{9}{16}\lambda \ln \lambda - 1.19358\lambda + 0.159317\lambda^3 + O(\lambda^4), \quad (15)$$

where $\lambda = r_s/h$. This is the apparent diffusivity based on a concentration difference between bulk solutions at the ends of the channel; that is, it includes the effect of steric partitioning between the channel and external solutions. For $h = 20$ nm and the range of Ficoll sizes used here, $0.15 \leq \lambda \leq 0.31$, so that $0.43 \leq D_{ch}/D_\infty \leq 0.66$. Using Eq. 15, the permeability of the slit channel is given by

$$k_{sc} = \frac{D_{sc}}{H}. \quad (16)$$

RESULTS

The Ficoll permeabilities measured for the intact capillary wall (k_{wall}) and the acellular capillary (k_{bare}) are shown in Fig. 4 and Table 1. As expected, both k_{wall} and k_{bare} decreased with increases in solute size. Moreover, for any given solute size, k_{bare} greatly exceeded k_{wall}.

In the intact capillary wall, most of the surface of the GBM is covered by cells, limiting the surface area available for paracellular diffusion. The exposed areas on the luminal and Bowman's space sides correspond to the endothelial fenestrae and epithelial filtration slits, respectively. The

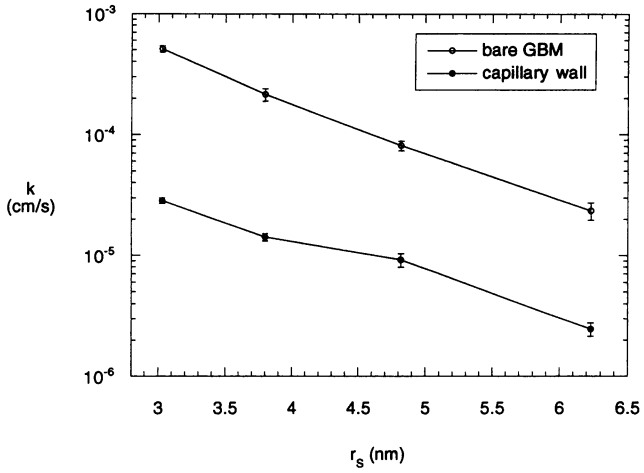

FIGURE 4 Ficoll permeability (k) of intact and acellular capillaries as a function of Stokes-Einstein radius (r_s). The results are shown as mean ± SE.

blockage of most of the GBM surface by cells results in tortuous rather than straight diffusion paths across the GBM, which tends to increase the concentration drop across this layer. Thus an indirect effect of the cell layers is to make the apparent diffusional resistance of GBM in the intact capillary wall greater than that for bare GBM. The increased diffusional resistance of the GBM is analogous to the increase in its resistance to water flow, which was analyzed in detail by Drumond and Deen (1994a). As described above, we estimate that $k_{GBM} = k_{bare}/2.33$, where k_{GBM} is the apparent permeability of the GBM within the intact capillary. Using the concept of resistances in series, the individual diffusional permeabilities for the intact capillary wall are related by

$$\frac{1}{k_{wall}} = \frac{1}{k_{GBM}} + \frac{1}{k_{cell}}, \quad (17)$$

where k_{cell} represents the combined contributions of the two cell layers. (As will be discussed, we assume that k_{cell} is determined almost entirely by the epithelial slit diaphragm.) The calculated values of k_{GBM} and k_{cell} are shown in Table 1. Even with the correction factor of 2.33 embedded in k_{GBM}, the cells still offered the greater resistance to diffusion. Nonetheless, the diffusional resistance of the GBM was not negligible. As shown in Fig. 5, the relative contribution of the GBM to the overall diffusional resistance increased with molecular size, from 13% at $r_s = 3.0$ nm to 26% at $r_s = 6.2$ nm.

For diffusion through a simple aqueous layer, the permeability will vary in proportion to the solute diffusivity in bulk solution (D_∞), so that k/D_∞ will be constant for all molecular sizes. As shown in Table 2, k_{bare}/D_∞ was found to decrease with increasing molecular size, confirming that the GBM offers size-dependent hindrances to diffusion. The cellular contribution to the permeability depended somewhat less strongly on molecular size than did that for GBM.

TABLE 1 Ficoll permeabilities for the glomerular capillary wall

r_s (nm)	k_{wall} (10^{-6} cm/s)	k_{bare} (10^{-6} cm/s)	k_{GBM} (10^{-6} cm/s)	k_{cell} (10^{-6} cm/s)
3.0	28.5 ± 1.5	508 ± 31	219 ± 13	33 ± 2
3.8	14.2 ± 1.0	214 ± 25	92 ± 11	17 ± 2
4.8	9.2 ± 1.2	81 ± 8	35 ± 3	12 ± 3
6.2	2.5 ± 0.3	24 ± 4	10 ± 2	3.3 ± 0.7

Results are given as mean ± SE. The number of experiments for each set of conditions ranged from 7 to 11.

That is, k_{cell}/D_∞ declined by a factor of ~5 over the range of molecular sizes studied, whereas k_{bare}/D_∞ (or k_{GBM}/D_∞) decreased by a factor of ~10. Consequently, the GBM resistance became a greater fraction of the total for larger molecular sizes, as already noted.

A more detailed examination of the factors that determine the permeability of the GBM reveals that

$$k_{bare} = \frac{\Phi D}{\delta} = \frac{\Phi K_d D_\infty}{\delta}, \qquad (18)$$

where Φ and D are the partition coefficient and diffusivity of the solute, respectively, in the GBM, and δ is the GBM thickness. The partition coefficient is defined here as the volume-averaged solute concentration in the GBM divided by that in the external solution, at equilibrium. The apparent diffusivity of a solute in the GBM, relative to that of an equivalent layer of water, is given by the factor ΦK_d, where $K_d = D/D_\infty$. Values of ΦK_d were calculated from k_{bare} and D_∞ by assuming a typical GBM thickness in the rat of δ = 200 nm (Daniels et al., 1993). The results are shown in Table 2. Whereas $\Phi K_d = 1$ corresponds to no steric or diffusional hindrances, the actual values in the GBM are roughly 10^{-2} to 10^{-3}. These low values indicate that the GBM does indeed represent a substantial barrier to diffusion. The results for ΦK_d are well represented by the empirical formula

$$\Phi K_d = 0.1045 \exp(-0.7302 r_s), \qquad (19)$$

where r_s is in nanometers. This expression should be used only within or near the range of molecular radii studied, $3.0 \le r_s \le 6.2$ nm.

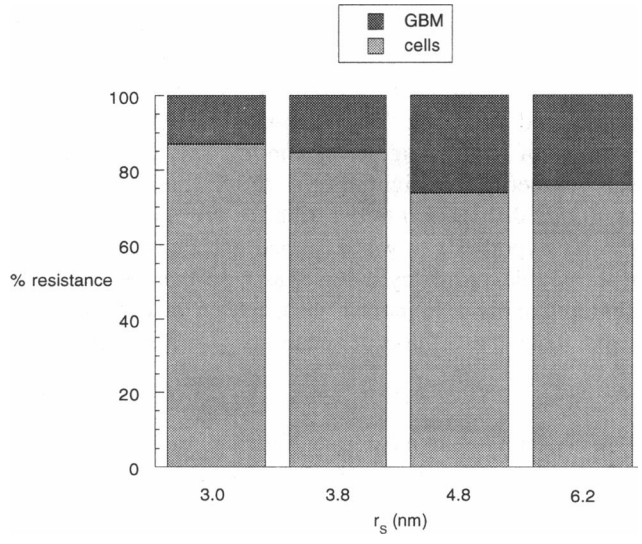

FIGURE 5 Relative resistances of the GBM and the cell layers to Ficoll diffusion across the glomerular capillary wall. The resistances were computed as reciprocals of the corresponding permeabilities.

DISCUSSION

This study provides the first direct measurements of the diffusional permeabilities of isolated, intact glomerular capillaries and GBM to well-characterized, nearly ideal test macromolecules of discrete size. In the previous application of our confocal microscopy technique, the diffusion data were limited to a polydisperse dextran (Daniels et al., 1993). In addition to covering a wide range of molecular sizes, the Ficoll fractions used here as test macromolecules offered two advantages: they were relatively monodisperse, and Ficoll (unlike dextran) diffuses through small pores at the rates expected for ideal, neutral spheres (Davidson and Deen, 1988). Thus a more definitive characterization of size-dependent restrictions to diffusion was possible. For any given size of Ficoll, a comparison of the permeabilities of intact and acellular glomerular capillary loops showed that the cell layers offered the dominant resistance to diffusion. This is in keeping with the conclusion reached in our previous study with dextran. Although the GBM was calculated to offer an average of only about 20% of the diffusional resistance of the intact capillary wall, it is by no means a negligible part of the barrier. Indeed, bare GBM was found to have a diffusional permeability ranging from about 10^{-2} to 10^{-3} times that of a layer of water of the same thickness, depending on molecular size.

TABLE 2 Size-dependent hindrances to diffusion in the GBM and cell layers

r_S (nm)	D_∞ (cm²/s)	k_{bare}/D_∞ (cm^{-1})	k_{cell}/D_∞ (cm^{-1})	ΦK_d
3.0	8.5×10^{-7}	596 ± 36	38 ± 3	1.2×10^{-2}
3.8	6.8×10^{-7}	314 ± 37	25 ± 3	6.3×10^{-3}
4.8	5.4×10^{-7}	151 ± 14	23 ± 5	3.0×10^{-3}
6.2	4.1×10^{-7}	57 ± 9	8 ± 2	1.1×10^{-3}

Results are given as mean ± SE. The values for ΦK_d are based on data for bare GBM.

The permeability properties of GBM are discussed in more detail in the companion paper (Edwards et al., 1997), in which additional data are presented concerning the hydraulic permeability and the size-dependent hindrances to the convective movement of Ficoll through this structure. In the remainder of the present discussion we focus on a possible structural basis for the cellular contribution to the diffusional resistance.

As already mentioned, it seems likely that the slit diaphragm is responsible for most of the cellular resistance to diffusion. Whichever structure in Fig. 2 is adopted to represent the slit diaphragm (zipper or ladder), an apparently inescapable conclusion is that the spacing of the cylindrical fibers is not uniform. Ficoll molecules approximately 12 nm in diameter (i.e., 6.2 nm Stokes-Einstein radius) were found here to diffuse across the intact glomerular capillary wall, and even larger Ficoll molecules appear in the urine of normal rats (Oliver et al., 1992). As already mentioned, previous structural, hydrodynamic, and diffusional data suggest that Ficoll closely resembles a rigid sphere (Davidson and Deen, 1988). Thus the transmural passage of these large Ficoll molecules is plainly inconsistent with uniform openings in the slit diaphragm of 4 × 14 nm, as in the zipper structure. The need to assume a nonuniform cylinder spacing in the ladder model also, based on glomerular sieving data in vivo, is discussed by Drumond and Deen (1995). In particular, suppose that the hydraulic permeability of the slit diaphragm is equal to that predicted for the zipper structure (i.e., 7.9×10^{-8} m s^{-1} Pa^{-1}; Drumond and Deen, 1994b). This value implies that the hydraulic resistances of the epithelium and GBM are approximately equal to one another in the intact capillary, and yields an overall hydraulic permeability that is consistent with micropuncture-based estimates for the rat glomerular capillary wall in vivo (Drumond and Deen, 1994a). To achieve this same hydraulic permeability with the ladder structure, assuming uniformly spaced cylinders with $r_c = 2$ nm, the required opening between the cylinders (corresponding to the quantity $2u$) is only 2.4 nm. Such small openings would preclude the passage of rigid spheres of even 2 nm radius, again in clear contradiction to experimental findings.

For the reasons just described, we assumed that in the slit diaphragm there is a distribution of gap half-widths, u. A lognormal distribution was used, characterized by a mean spacing (u_m) and a parameter that describes the variance of the spacing (s). The hydraulic permeabililty of the slit diaphragm was fixed at the value given above, so that only one of these parameters could be varied independently. The independent parameter in the lognormal distribution was chosen as s, so that the slit diaphragm structure was characterized by r_c, s, and the hydraulic permeability. Drumond and Deen (1995) used a gamma distribution for the half-widths, which yields qualitatively similar results.

We first examined the theoretical effects on k_{cell} of varying r_c and s, with the hydraulic permeability of the slit diaphragm fixed. Results are given in Fig. 6 for $r_c = 2$ or 4 nm, and s ranging from 1.5 to 2.0. All of the curves in this

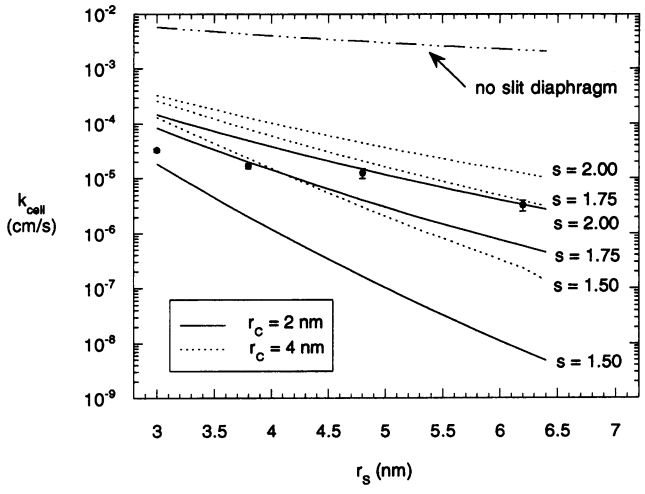

FIGURE 6 Measured and theoretical values of the cellular permeability to Ficoll, assumed to equal the permeability of the epithelial filtration slit. Theoretical results for intact slit diaphragms are shown for two values of the cylinder radius (r_c) and three values of the parameter that describes the breadth of the lognormal distribution of cylinder spacings (s). Theoretical results are shown also for a hypothetical situation in which the slit diaphragm is absent.

semilogarithmic plot are roughly linear. In response to selective increases in either s or r_c, the slopes decrease and the absolute values of k_{cell} increase. Also shown in Fig. 6 are the measured values of k_{cell}. Although the data are within the overall range of the theoretical curves, it is seen that for parameter combinations which give the correct order of magnitude for k_{cell}, the slopes predicted by the hindered diffusion model are much too large. In other words, the data show much less size selectivity than is expected for a structure with the hydraulic permeability that has been inferred for the slit diaphragm.

A possible explanation for the discrepancy between the predicted and measured values of k_{cell} is that, in addition to a continuous (lognormal) distribution of cylinder spacings, there were small areas devoid of cylinders. It must be emphasized that such "missing rungs" are not necessarily evidence of any damage to or abnormality in the capillary wall. Rather, they might simply reflect the inability of a lognormal distribution to describe the normal structure. To test this hypothesis, it was assumed that the fractional area of the slit devoid of cylinders was f, so that the fractional area containing a lognormal distribution of cylinders was $1 - f$. Thus the cellular permeability was given by

$$k_{cell} \cong k_{ep} = \epsilon_s[(1-f)(k_{sd}^{-1} + k_{sc}^{-1})^{-1} + fk_{sc}], \quad (20)$$

where k_{sd} and k_{sc} are the permeabilities of the slit diaphragm and slit channel, respectively, based on the cross-sectional area of a single filtration slit. The factor ϵ_s, which is the fraction of the basement membrane area in contact with filtraton slits, is needed because k_{cell} and the epithelial permeability k_{ep} are based on total surface area rather than slit area. It is seen that if the slit diaphragm is assumed to be

absent (i.e., $f = 1$), the diffusional permeability of the slit will equal that of the open channel. As shown by the curve in Fig. 6 labeled "no slit diaphragm," k_{cell} in this case would have a smaller slope, and much larger absolute values, than the experimental data. Thus it appears that a very small value of f might be sufficient to account for the experimental results.

To determine the values of r_c, s, and f that provided the best fits to the data for k_{cell}, we minimized the error measure given by

$$\chi^2 = \sum_{i=1}^{4} \left(\frac{\ln(y_i/z_i)}{\ln \sigma_i} \right)^2, \quad (21)$$

where y_i and z_i are the measured and calculated values of k_{cell}, respectively, for Ficoll fraction i, and σ_i is the standard deviation of y_i. Logarithms were employed in the sum of squares because of the wide (10-fold) range of k_{cell}. Powell's method (Press et al., 1989) was used for the nonlinear parameter estimation. Preliminary calculations revealed that small values of r_c (<1 nm) tended to give the best fits to the permeability data. However, as discussed by Drumond and Deen (1995), values of $r_c < \sim 2$ nm are inconsistent with the range of slit diaphragm thicknesses estimated from electron micrographs in several published studies. For example, the bridge fibers reported by Rodewald and Karnovsky (1974) have a radius of 3.5 nm. Accordingly, we chose to fix r_c at 1.0, 2.0, or 4.0 nm. Fits were performed by allowing s to vary with $f = 0$, or by allowing both s and f to vary.

The parameter values calculated for the slit diaphragm are shown in Table 3. As expected, allowing f to be nonzero provided much better fits to the data. This was true for all choices of r_c, as shown by the values of χ^2 in Table 3 and by the plots of k_{cell} in Fig. 7. Based on an F test (Motulsky and Ransnas, 1987), the improvements in the fits to the k_{cell} data with $f \neq 0$ were greater than could have been expected by increasing the number of adjustable parameters from 1 to 2. With or without postulated areas devoid of cylinders, the model predictions for r_c values of 1.0, 2.0, and 4.0 nm were quite similar. For all cases, the best-fit value of f was ~0.002. That is, the area devoid of cylinders was inferred to be tiny, only ~0.2% of the slit area.

An important feature of the present experiments is that the fluorescence measurements were so localized that any one permeability determination was affected by a very small number of filtration slits. A critical examination of the slit diaphragm model requires some consideration of the anatomical implications of the best-fit parameter values. The filtration slits extend around the circumference of the capillaries, the slit diaphragm being located typically at a diameter of ~8 μm. Accordingly, the total length of a single, idealized slit diaphragm is ~25 μm. The average center-to-center distance between the cylindrical fibers is $2(u_m + r_c)$, so that, taking $r_c = 2$ nm and $u_m = 1$ nm as an example (Table 3), the length occupied by the average unit is 6 nm. Thus the number of openings in one slit diaphragm is calculated to be extremely large, (25 μm)/(6 nm) = 4×10^3. This justifies the use of a continuous (e.g., lognormal) probability distribution for the cylinder spacings in the model. With $f = 0.002$, the length of the perimeter where cylinders are absent is only 0.002×25 μm = 50 nm, a space equivalent to that needed by ~8 average units. This emphasizes how a seemingly small supplement to the tail of the lognormal distribution can significantly reduce the slope of a plot of k_{cell} versus r_s. Similar conclusions are reached if it is assumed that $r_c = 1$ or 4 nm. Given the consistency of the permeability results from one experiment to another, it appears that the same structural features were present, to only a slightly varying degree, in the slit diaphragms of all regions examined. The value $f = 0.002$ cannot be explained, for example, by postulating that two of every thousand slit diaphragms were completely absent. Moreover, it seems unlikely that there was random damage to the slit diaphragms due to the experimental procedure, in that the hydodynamic model predicts that even small areas of damage would yield order-of-magnitude variations in the measured values of k_{cell} from glomerulus to glomerulus.

The probability density that describes the distribution of cylinder spacings, $g(u)$, is plotted in Fig. 8 for the intermediate value of $r_c = 2$ nm. As can be seen, the distribution is fairly narrow. Thus, if this structural interpretation is cor-

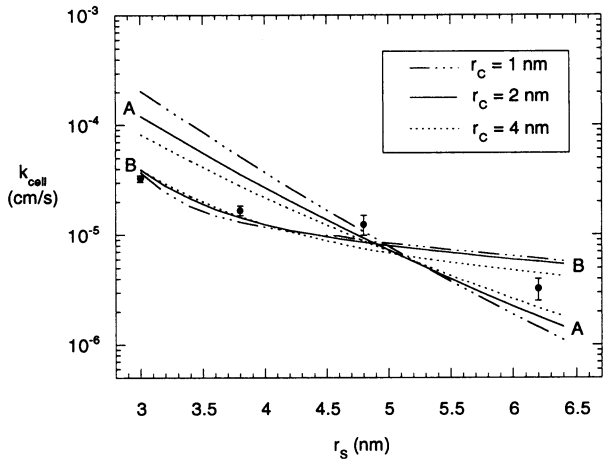

FIGURE 7 Measured and theoretical values of the cellular permeability to Ficoll, interpreted as the permeability of the filtration slit. The theoretical curves labeled A were drawn assuming that the cylinder spacings in the slit diaphragm follow a lognormal distribution. The curves labeled B were drawn assuming that, in addition to the lognormal distribution, a small area is devoid of cylinders. The calculated values were obtained by assuming a cylinder radius of 1, 2, or 4 nm, and fitting the parameters s and f to the data (see text and Table 3).

TABLE 3 Parameter values calculated for the slit diaphragm

r_c (nm)	1.0	1.0	2.0	2.0	4.0	4.0
s	2.20	1.82	1.89	1.53	1.63	1.30
f	0	0.0020	0	0.0026	0	0.0028
u_m (nm)	0.40	0.55	0.75	0.98	1.33	1.62
$\chi^2 \times 10^2$	0.56	0.16	1.09	0.19	2.15	0.22

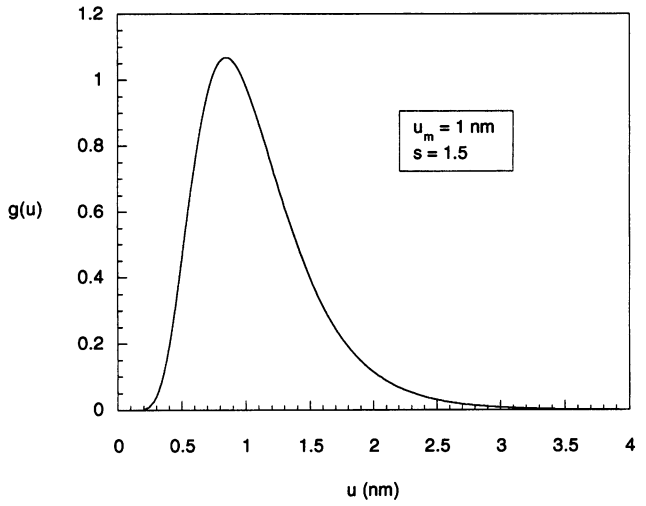

FIGURE 8 Probability density describing a lognormal distribution of cylinder spacings. The parameters used are those for r_c = 2 nm and $f \neq 0$ in Table 3 (rounded off).

rect, the examination of a few, randomly sampled images of the slit diaphragm might well give the impression of almost uniform cylinder spacings. Moreover, given the low value calculated for f, the probability of encountering an area devoid of cylinders would be quite low. It appears that an extensive investigation of high-resolution electron micrographs of slit diaphragms would be required to confirm or disprove our structural model.

In studies of frog mesenteric capillaries, Adamson and Michel (1993) observed 150-nm interruptions in the junction strand of the endothelial cleft, and these large breaks were found to be separated by at least 2000 nm. The electron micrographs also suggested a 2-nm-wide continuous slit in the tight junction. The large-orifice, narrow-slit model developed subsequently by Fu et al. (1994, 1995) for transport across this structure was consistent with both hydraulic conductivity and solute permeability data for mesenteric endothelium. As shown by Fu et al. (1995), in the presence of large discontinuities the lateral spreading of the diffusive tracer behind the breaks should be considered; our simplified approach for describing missing rungs in the slit diaphragm does not account for this effect. Another opportunity for improvement in the model would be to consider more accurately fluid flow through such interruptions, using an approach like that of Zeng and Weinbaum (1994) for Stokes flow through rectangular orifices in a channel. Given the limitations of our model, the quantitative estimates of the parameter f should be viewed with caution.

Molecular charge has been shown to be an important determinant of the selectivity of the glomerular barrier to macromolecules in vivo, the passage of negatively charged molecules normally being more restricted than that of neutral molecules of similar size and chemical structure (Maddox et al., 1992). It has been suggested that the GBM is a prominent part of the barrier to anionic macromolecules (Rennke et al., 1975; Bray and Robinson, 1984; Kanwar and Venkatachalam, 1992), although recent data support the opposite conclusion (Daniels, 1994). Future studies are needed to characterize the charge selectivity of the GBM in diffusion.

In summary, we measured the diffusional permeabilities of intact and acellular glomerular capillaries to Ficoll of varying molecular size. The cellular part of the resistance to diffusion, which we attribute largely to the epithelial slit diaphragm, was found to greatly exceed that of the GBM. A novel hydrodynamic model was developed to relate the cellular part of the diffusional resistance to proposed structures for the slit diaphragm. The data were most consistent with a ladder-like structure having a distribution of rung spacings, together with occasional regions devoid of rungs.

Excellent technical assistance was provided by Michael Ahlquist.

This work was supported by grants from the National Institutes of Health (DK20368 and DK45058). BD is the recipient of an American Heart Association Established Investigatorship.

REFERENCES

Adamson, R. H., and C. C. Michel. 1993. Pathways through the intercellular clefts of frog mesenteric capillaries. *J. Physiol.* 466:303–327.

Bray, J., and G. B. Robinson. 1984. Influence of charge on filtration across renal basement membrane films in vitro. *Kidney Int.* 25:527–533.

Daniels, B. S. 1994. Determinants of charge selectivity of the glomerular permeability barrier. *J. Lab. Clin. Med.* 124:224–230.

Daniels, B. S., W. M. Deen, G. Mayer, T. Meyer, and T. H. Hostetter. 1993. Glomerular permeability barrier in the rat: functional assessment by in vitro methods. *J. Clin. Invest.* 92:929–936.

Daniels, B. S., E. H. Hauser, W. M. Deen, and T. H. Hostetter. 1992. Glomerular basement membrane: in vitro studies of water, and protein permeability. *Am. J. Physiol.* 262(*Renal Fluid Electrolyte Physiol.* 31): F919–F926.

Davidson, M. G., and W. M. Deen. 1988. Hindered diffusion of water-soluble macromolecules in membranes. *Macromolecules.* 21: 3474–3481.

Drumond, M. C., and W. M. Deen. 1994a. Structural determinants of glomerular hydraulic permeability. *Am. J. Physiol.* 266 (*Renal Fluid Electrolyte Physiol.* 35):F1–F12.

Drumond, M. C., and W. M. Deen. 1994b. Stokes flow through a row of cylinders between parallel walls: model for the glomerular slit diaphragm. *J. Biochem. Eng.* 116:184–189.

Drumond, M. C., and W. M. Deen. 1995. Hindered transport of macromolecules through a single row of cylinders: application to glomerular filtration. *J. Biomech. Eng.* 117:414–422.

Edwards, A., B. S. Daniels, and W. M. Deen. 1997. Hindered transport of macromolecules in isolated glomeruli. II. Convection and pressure effects in basement membrane. *Biophys. J.* 72:000–000.

Fu, B. M., F. E. Curry, and S. Weinbaum. 1995. A diffusion wake model for tracer ultrastructure-permeability studies in microvessels. *Am J. Physiol.* 269(*Heart Circ. Physiol.* 38):H2124–H2140.

Fu, B. M., S. Weinbaum, R. Y. Tsay, and F. E. Curry. 1994. A junction-orifice-fiber entrance model for capillary permeability: application to frog mesenteric capillaries. *J. Biomech. Eng.* 116:502–513.

Hora, K., S. Ohno, H. Oguchi, T. Furukawa, and S. Furuta. 1990. Three-dimensional study of the glomerular slit diaphragm by the quick-freezing, and deep-etching replica method. *Eur. J. Cell Biol.* 53: 402–406.

Johnson, E. M., D. A. Berk, R. K. Jain, and W. M. Deen. 1996. Hindered diffusion in agarose gels: test of effective medium model. *Biophys. J.* 70:1017–1026.

Kanwar, Y. S., and M. A. Venkatachalam. 1992. Ultrastructure of glomerulus, and juxtaglomerulus apparatus. *In* Handbook of Physiology. Renal Physiology, Sect. 8, Vol. 1. American Physiological Society, Bethesda, MD. 3–40.

Ligler, F. S., and G. B. Robinson. 1977. A new method for the isolation of renal basement membrane. *Biochim. Biophys. Acta.* 468:327–340.

Maddox, D. A., W. M. Deen, and B. M. Brenner. 1992. Glomerular filtration. *In* Handbook of Physiology. Renal Physiology, Sect. 8, Vol. 1. American Physiological Society, Bethesda, MD. 545–638.

Motulsky, H. J., and L. A. Ransnas. 1987. Fitting curves to data using nonlinear regression: a practical and nonmathematical review. *FASEB J.* 1:365–374.

Oliver, J. D., S. Anderson, J. L. Troy, B. M. Brenner, and W. M. Deen. 1992. Determination of glomerular size selectivity in the normal rat with Ficoll. *J. Am. Soc. Nephrol.* 3:214–228.

Pawar, Y., and J. L. Anderson. 1993. Hindered diffusion in slit pores: an analytical result. *Ind. Eng. Chem. Res.* 32:743–746.

Press, W. H., B. P. Flannery, S. A. Teukolsky, and W. T. Wetterling. 1989. *Numerical Recipes*. Cambridge University Press, New York.

Rennke, H. G., R. S. Cotran, and M. A. Ventkatachalam. 1975. Role of molecular charge in glomerular permeability. *J. Cell. Biol.* 67:638–646.

Rodewald, R., and M. J. Karnovsky. 1974. Porous substructure of the glomerular slit diaphragm in the rat and mouse. *J. Cell Biol.* 60: 423–433.

Zeng, Y., and S. Weinbaum. 1994. Stokes flow through periodic orifices in a channel. *J. Fluid Mech.* 263:207–226.